Use of 3D-printed mixers in laboratory reactor design for modelling of heterogeneous catalytic converters

Chemical Engineering & Processing: Process Intensification 164 (2021) 108325

Contents lists available at ScienceDirect

Chemical Engineering and Processing - Process Intensification

journal homepage: www.elsevier.com/locate/cep

Use of 3D-printed mixers in laboratory reactor design for modelling of heterogeneous catalytic converters

Magnus Walander [a,*], Andreas Nygren [a], Jonas Sjöblom [a,*], Emil Johansson [b], Derek Creaser [c], Jonas Edvardsson [d], Stefanie Tamm [d], Björn Lundberg [e]

[a] Mechanics and Maritime Sciences, Chalmers University of Technology, Gothenburg, Sweden
[b] RISE IVF AB, Mölndal, Sweden
[c] Chemistry and Chemical Engineering, Chalmers University of Technology, Gothenburg, Sweden
[d] Johnson Matthey, Gothenburg, Sweden
[e] Volvo Cars Corporation, Gothenburg, Sweden

ARTICLE INFO

Keywords:
Reactor design
Radial mixing
Axial dispersion
Step experiment
3D-printing
Static mixer

ABSTRACT

A method for identifying radial concentration maldistribution in synthetic catalyst activity test (SCAT) benches, is presented, where spatially resolved concentration measurements are not available. The developed methodology was successfully tested for an injection-based SCAT. To resolve the radial concentration maldistribution a static mixer was designed, 3D-printed and inserted upstream the test sample. The methodology could also prove the effectiveness of the mixer, which did not only resolve the concentration maldistribution but also avoided causing reaction disturbances. The resulting increased axial dispersion from the turbulence created by the static mixer was evaluated using a 3D CFD model in Ansys Fluent 19. The axial dispersion of the injection-based SCAT bench was compared to a premixed SCAT bench through classical Aris-Taylor calculations. The results from the axial dispersion calculations show that the injection-based design with the use of a static mixer is far superior to the premixed design – both with regards to pulse broadening but also time delay. This is highly desirable for modelling studies towards zero emission exhaust aftertreatment.

1. Introduction

Monolithic catalysts are used in a wide range of processes due to their compact nature, low pressure drop and high specific surface area when coated [1]. Their most common application is within the automotive industry within exhaust aftertreatment systems (EATS), where hazardous emissions produced by internal combustion engines are removed [2]. Due to increasingly stringent automotive emission legislations modelling of the EATS and its components can help with EATS development. Due to the vast range of scales (~0.1 m to ~1 nm) of processes occurring in a monolithic reactor, the most common way to reduce computational cost is to limit the reactor model to a single channel within the monolith [3–5]. This assumes that all channels, no matter the radial position, have identical inlet conditions – including; volumetric flow rate, temperature and gas composition. In a large-scale, practical applications, these assumptions are not realistic since the piping before the EATS often includes various sharp bends leading to different volumetric flow rate in each channel [6]. However, for modelling purposes of lab-scale catalysts, it is vital that these boundary conditions are fulfilled and verified. Erroneous assumptions in inlet conditions could lead to e.g. incorrectly estimated kinetics or noble metal dispersion measurements.

1.1. Laboratory reactor design

There are two common ways of designing a synthetic catalyst activity test (SCAT) bench with regards to controlling the inlet conditions but also the operation of the test bench itself. The designs are compared with regards to satisfaction of the previously mentioned single channel assumptions, but also with regards to suitability for use in concentration step change experiments, which are valuable for kinetic modelling

Abbreviations: ABS, Acrylonitrile Butadiene Styrene; CFD, Computational Fluid Dynamics; CPSI, Cell Per Square Inch DLP; DLP, Digital Light Processing; DMD, Digital Micromirror Device; DOC, Diesel Oxidation catalyst; EATS, Exhaust AfterTreatment System; MFC, Mass Flow Controllers; SCAT, Synthetic Catalyst Activity Test.

* Corresponding authors.
E-mail addresses: magwal@chalmers.se (M. Walander), jonas.sjoblom@chalmers.se (J. Sjöblom).

https://doi.org/10.1016/j.cep.2021.108325
Received 10 September 2019; Received in revised form 28 September 2020; Accepted 26 January 2021
Available online 2 February 2021

Nomenclature

$A_i[m^2]$	Area for segment i
$A_{tot}[m^2]$	Total area
$C[-]$	Tracer concentration
$C_{t_0}[-]$	Initial Concentration
$C_{t_\infty}[-]$	Final Concentration
$D_{AB}[m^2/s]$	Molecular diffusivity
$D_{eff}[m^2/s]$	Effective axial dispersion coefficient
$D_{eff,\,turb}[m^2/s]$	Turbulent effective axial dispersion coefficient
$D_t[m]$	Pipe diameter
erf	Error function
$f[-]$	Fluid friction factor
$h(t)[-]$	Transfer function
$Re[-]$	Reynolds number
$t[s]$	Time
$\overline{u}[m/s]$	Mean fluid velocity
$x(t)[-]$	Input signal
$y(t)[-]$	Output signal
$Z[m]$	Axial coordinate

Greek letters

$\gamma[-]$	Uniformity index
$\nu[m^2/s]$	Kinematic viscosity
$\psi_{avg}[-]$	Area weighted average state variable value
$\psi_i[-]$	Sate variable value for segment i

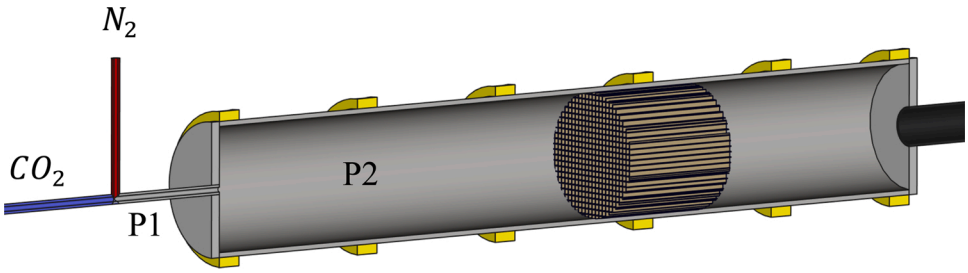

Fig. 1. Drawing of a typical premixed SCAT bench design. The carrier gas (red piping) are mixed with reactants (blue piping) in a T-junction. The mixed gases travel through a pipe (part P1) to enter the preheater (part P2). The preheater itself is a tube, surrounded by a heating coil (yellow), where the catalyst sample is placed. The entire outflow of the catalyst sample is sampled (black pipe) for determining temperature and species concentration. (For interpretation of the references to colour in this figure legend, the reader is referred to the web version of this article).

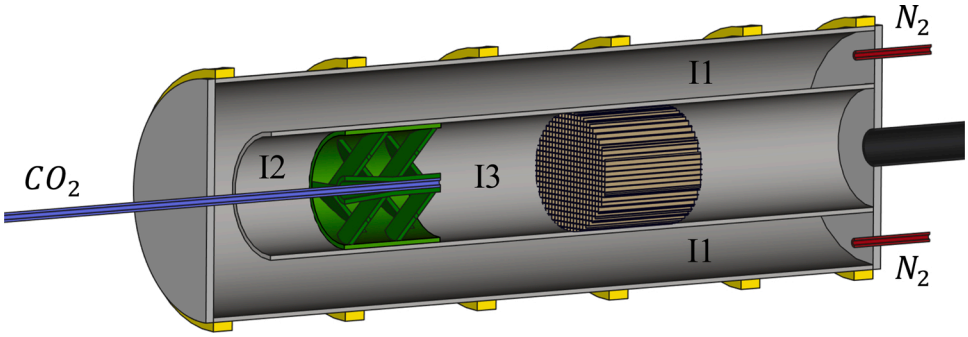

Fig. 2. The carrier gas (red piping) enter an outer cylinder (part I1), where they are heated by an electrically heated coil. The carrier gas travels to the other side of the SCAT bench where it enters the inner cylinder (part I2). The reactants (blue piping) are injected, through a set of capillaries, and mix with the carrier gas (part I3). The mixture enters the catalyst sample. The entire outflow of the catalyst sample is sampled (black pipe) for determining temperature and species concentration. (For interpretation of the references to colour in this figure legend, the reader is referred to the web version of this article).

studies [7]. Even though there are mathematical ways of treating perturbed transients in experimental data [8], it is clearly easier to avoid them to begin with. Hence, the design should minimize perturbation of ideal steps through axial dispersion.

1.1.1. Premixed reactant flow test bench

The conventional premixed reactant flow test bench is depicted in Fig. 1. As the name suggests, a series of independently controlled mass flow controllers (MFC) mix the carrier gas (red piping) with the reactants (blue piping) in a T-joint. The gas mixture travels through a pipe (part P1) until they enter a preheater. The entrance to the preheater typically involves a sudden area enlargement that would contribute to an increased axial dispersion because of the likely vortex formation in the corners. However, this effect can easily be limited by smoothening out the corners of the entrance, and so its contribution is neglected in this paper (the sudden area enlargement after the mixing point is only for illustration purposes). The preheater (part P2) usually consists of a tube with the same diameter as needed for the catalyst sample, surrounded by a heated coil (yellow). The premixed gases are heated to a designated inlet temperature before entering the test monolith itself. Lastly, the mixed-cup concentration and temperature is measured (black piping) using various types of analyzers.

1.1.2. Injection-based test bench

The other test bench design can be seen in Fig. 2. In contrast to the premixed design, the injection-based test bench consists of a large oven. The carrier gas is injected into an outer cylinder (part I1) where it is preheated by an electrically heated coil (yellow). The carrier gas flows to the other end of the SCAT bench where it enters an inner cylinder (part I2). In the inner cylinder, the reactants are injected through a set of capillaries. The reactants mix with the carrier gas through radial diffusion (part I3) and the gas mixture enter the catalyst sample. Again, the mixed-cup concentration and temperature is measured (black piping) using various types of analyzers. The positioning of the proposed mixer (green) further described in section 2.2 is also shown here.The injection-based test bench design allows for some advantageous features. For one, due to the carrier gas flowing in a two-pass configuration around the inner cylinder where the catalyst sample is located, the operation could

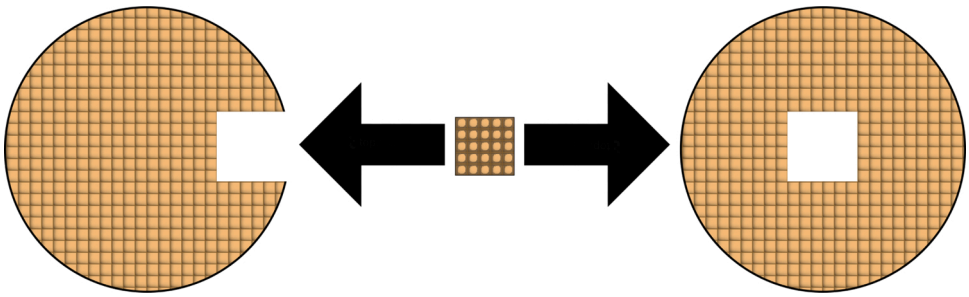

Fig. 3. Illustration of the prepared samples. From left: Empty monolith with 6 × 6 channel cutout at the edge. 5 × 5 channel active core placed in each empty monolith. Empty monolith with 6 × 6 channel cutout in the center.

be considered as adiabatic – helping to remove any unwanted radial and axial temperature gradients. This could technically be achieved with the premixed design as well, though a longer piping with premixed reactants would mean higher axial dispersion – which, again, is desirable to minimize. This risk is eliminated with the injection-based design because there is no axial dispersion in the capillaries since the reactants are not yet diluted. Furthermore, since all the reactants necessary for reactions are present in the piping in the premixed design – hot surfaces and contamination could cause unwanted reactions. Again, this is more or less eliminated with the injection-based design where all reactants are flowing in separate capillaries until a short distance upstream the catalyst sample. However, because of the short distance between the injection point and the catalyst sample along with a usually laminar flow profile, there is a risk of having a radial concentration gradient as the reactants enter the monolith due to insufficient time for mixing by radial diffusion. It should be stressed that if the experiments are only of steady-state type, the premixed design is inherently better as axial dispersion is not an issue for steady-state measurements; it allows for a guaranteed well-mixed flow and its potential temperature gradients can be improved by utilizing the two-pass flow configuration.

The problem is that the outlet concentration of the catalyst sample is usually measured as a mixed-cup and therefore any radial maldistributions may never be discovered as it is not certain that a concentration maldistribution will lead to a significant change conversion compared to a well-distributed one. At least if there is only one injected reactant, e.g. carbon monoxide, which is maldistributed and the carrier gas and oxygen is well mixed. Some channels will show higher reactivity while others have lower and the average conversion is equal to that of a well-distributed case.

This might also hold true for a reaction where two reactants are injected, e.g. ammonia and nitrogen oxides. As long as they share the same maldistribution, the observed conversion will be the equal to that of a well-distributed case. That is, unless the operation is kinetically controlled, then the well-mixed case should show higher conversion. However, as different reactants have different diffusivities, their respective maldistribution will likely differ from each other – and so it is important to develop an experimental method to identify these gradients.

To solve a possible radial concentration maldistribution as a result of gas/gas injection, there is literature readily available on the use of static mixers in pipe flow [9–11]. However, these articles only touch upon steady-state operation and the mixers are usually developed for turbulent conditions when it comes to gas/gas injection. For kinetic studies the mixer should also be non-reactive, have no adsorption of reactants, give rise to as little axial dispersion as possible and withstand highly transient temperature ramps without cracking.

In this paper, an innovative way of identifying possible radial concentration maldistributions within an injection-based SCAT bench, *without* the possibility of measuring the concentration locally, has been developed. To resolve the *observed* concentration maldistribution, a static mixer design has been developed with objectives of firstly resolving the radial concentration gradient for common operating conditions and secondly minimizing axial dispersion and facilitating ease of use on a daily basis. The static mixer was 3D-printed in a single piece, in various materials, to allow for complex and rapid iterations in design. The final mixer was 3D printed in dense α-alumina which exhibit a high chemical resistance and a high thermal stability suitable for the SCAT bench tests. The axial dispersion of the premixed design is compared to the injection-based design through Aris-Taylor dispersion calculations and CFD simulations of the static mixer.

2. Material and methods

2.1. SCAT core experiments

Because of accessibility limitations, the analyzers in the injection-based SCAT bench only measures bulk averaged concentration. Therefore, it is difficult to identify large but local gradients in concentration near the inlet of the monolith. As a solution, a core of 5 × 5 channels was cutout from a 1 in long 400 cpsi diesel oxidation catalyst (DOC) monolith, coated with 30 g Pt/ft^3 of monolith. The DOC core was then suspended in two different radial positions (in the center and at the edge) within uncoated 1 × 1 inch monoliths. A schematic picture of the two prepared samples can be seen in Fig. 3. Note that the exact same active 5 × 5 channel core was used in each radial position.

Each sample was then subject to short concentration step experiments using 0–100 or 0–1000 ppm of propene in a steady flow of 8 % oxygen in 20 L_N/min (space velocity, SV = 128000 h^{-1}, same for both the entire sample and the active core) or 40 L_N/min (404000 h^{-1}, same for both the entire sample and the active core) of nitrogen as carrier gas. The short duration of the pulses counteracts a change in noble metal oxidation state, which if present would obstruct easy analysis of the results. Each step was repeated for calculation of standard deviation and each set of steps was repeated for a number of temperatures. The steady state part of the step (at high concentration) was used to calculate the conversion. If the conversion depends on the radial positioning of the active DOC core, then there is a local difference in inlet concentration. Hence a static mixer is needed for resolving the radial concentration maldistribution. After the mixer is positioned in the SCAT bench upstream the active core, the experiments are repeated. The experiments are also repeated with a completely empty SCAT bench as well as mixer only to identify whether the laboratory reactor shows reactivity without catalyst sample or if the mixer shows reactivity or adsorption.

2.2. Mixer design

The mixer used in this paper was developed at Chalmers University of Technology through iterative testing. The mixer was initially 3D-printed in ABS plastic and tested in a small-scale version of the injection-based SCAT bench. The mixer was tested using injection of pure carbon dioxide gas (tracer) into nitrogen gas (carrier) at room temperature. The carbon dioxide concentration was measured in

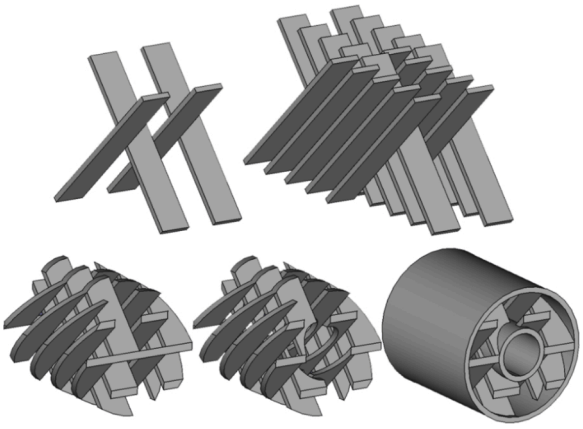

Fig. 4. Illustrative assembly of the mixer. Top row from left: 4 cross-bars (N_x) over the width of the channel (radially). 5 parallel crossbars (N_p) across the unit length (axially). Bottom row from left: Assembled matrix cutoff by geometry of channel. Assembled matrix with cutout center-hole for a thermocouple and capillaries for injection of reactants. Completely assembled mixer with housing.

varying radial and tangential positions downstream the mixer using a capillary connected to a carbon dioxide analyzer. Variations of the static mixer were tested for varying tracer concentration and carrier volumetric flow rates. The design is closely based on the SMX mixer presented by Singh et al. [9], along with their suggested design equations. One early design modification was to allow for a thermocouple, measuring monolith inlet temperature, to be inserted straight through the mixer without interfering with mixing. Additionally, to avoid unwanted tracer adsorption onto the mixer itself and facilitate ease of use, the final mixer combined the matrix from the SMX with the injection idea of a plate type mixer. This means that the injection point is located in the turbulent wake behind the mixer, thus decreasing the risk of adsorption onto the mixer itself. The illustrative assembly of the mixer and its components is shown in Fig. 4.

2.3. 3D-printing of ceramic mixer

The final mixer design was manufactured in α-alumina by 3D printing at Research Institutes of Sweden (RISE) using a Cerafab 7500 stereolithography apparatus from Lithoz GmbH, Vienna, Austria. The equipment allows manufacturing of ceramic green parts, layer by layer, by selective photopolymerization of a ceramic suspension containing photoinitiator, crosslinking polymer resin and a high solid loading of a submicron ceramic powder. The system is based on Digital Light Processing (DLP) and uses a Digital Micromirror Device (DMD) with a resolution of 1920 × 1080 pixels, resulting in a high lateral resolution of 40 × 40 μm in the build plane. The light source is an array of 460 nm blue light LEDs. After manufacturing, the crosslinked polymer network was removed thermally by slowly heating the part up to 450 °C in air over 24 h. Finally, the temperature was increased at 5 °C/min to 1600 °C and the powder compact sintered for 2 h in order to form a dense alumina part.

3. Theory/calculation

3.1. Axial dispersion in the premixed design

The flow conditions in the premixed SCAT design varies from room temperature conditions with turbulent flow to high temperature conditions with laminar flow. This leads to distinct differences in the axial dispersion coefficient. Hence, dispersion calculations must be divided into two parts shown in Fig. 1; the turbulent part (P1) and the laminar part (P2) where the flow is gradually heated. The dispersion model is a simple material balance [12]:

$$\frac{\partial C}{\partial t} = D_{eff}\frac{\partial^2 C}{\partial Z^2} - \overline{u}\frac{\partial C}{\partial Z} \tag{1}$$

where C $[-]$ is the normalized tracer concentration, D_{eff} $[m^2/s]$ is the effective axial dispersion coefficient, Z $[m]$ is the axial coordinate and $\overline{u}$ $[m/s]$ is the mean fluid velocity. Its analytical solution for a step change input is:

$$C(t) = C_{t_0} + \left(C_{t_\infty} - C_{t_0}\right)\cdot\frac{1}{2}\left[1 - \mathrm{erf}\left(\frac{Z - \overline{u}t}{\sqrt{4D_{eff}t}}\right)\right] \tag{2}$$

where C_{t_0} $[-]$ is the initial concentration, C_{t_∞} $[-]$ is the final concentration, t $[s]$ is time and *erf* is the error function. For the turbulent flow in the smaller pipe at room temperature, the axial dispersion is calculated according to a correlation by Taylor [13]:

$$D_{eff,\,turb} = 3.57\overline{u}D_t\sqrt{f} \tag{3}$$

where D_t $[m]$ is the pipe diameter and f $[-]$ is the fluid friction factor. Since the exact roughness of the pipes are unknown, the Blasius correlation for smooth pipes is used [13]:

$$f = 0.079\ (Re)^{-1/4} \tag{4}$$

where Re $[-]$ is Reynolds number:

$$Re = \frac{\overline{u}D_t}{\nu} \tag{5}$$

where ν $[m^2/s]$ is the bulk kinematic viscosity. For the laminar flow in the preheater, the axial dispersion coefficient changes because the increase in molecular diffusivity and the accelerating flow. To calculate the overall dispersion, the pipe is discretized into multiple axial segments. Even though the conditions change, all segments fall into the Aris-Taylor dispersion regime. Hence the axial dispersion for each segment is calculated as [12]:

$$D_{eff,i} = D_{AB} + \frac{\overline{u}^2 D_t^2}{192 D_{AB}} \tag{6}$$

where D_{AB} $[m^2/s]$ is the molecular diffusivity of the tracer in the carrier gas. The overall dispersion effect can be solved by forward convolution as described later, putting the output of each segment as the input for the next.

3.2. Forward convolution

For any linear time-invariant system the output signal is the convolution of the input signal and the systems transfer function [8]:

$$y(t) = h(t) * x(t) \tag{7}$$

where $y(t)$ $[-]$ is the output signal (outlet concentration), $h(t)$ $[-]$ is the transfer function and $x(t)$ $[-]$ is the input signal (inlet concentration). In the case of a step change function as input, which is the case for the analytical solution in equation [2], the transfer function is the derivative of the output signal, i.e. the outlet concentration differentiated with respect to time. The transfer function for each part of the pipe is obtained numerically in MATLAB. Finally, a Dirac-delta (instantaneous pulse) is inserted as initial input signal and the built-in function *conv* is used to consequently convolute the signal with each transfer function. The overall dispersion effect for the premixed system is then compared with that of the injection-based system.

3.3. Axial dispersion in the injection-based system with mixer

To evaluate the transient behaviour of the mixer, a 3D CFD model was made using Ansys Fluent 19. The fluid domain of the mixer was

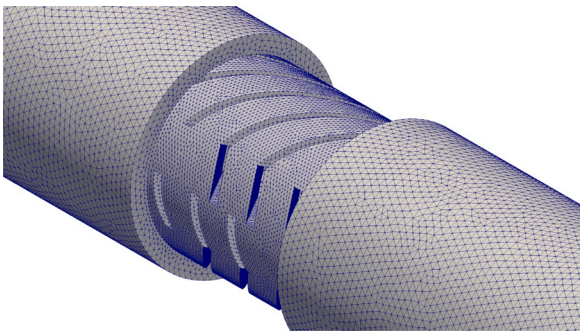

Fig. 5. Close-up of the CFD mesh of the fluid domain near the mixer.

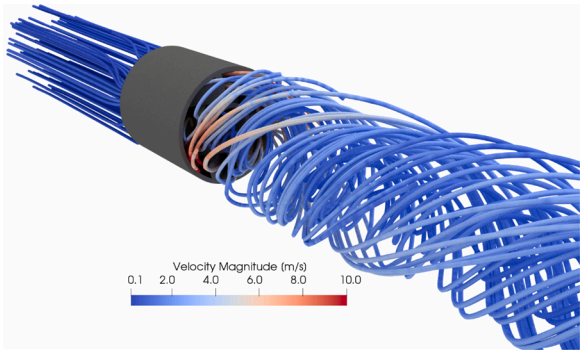

Fig. 6. Streamlines colored by velocity magnitude for CFD simulation of 20 L_N/min at 350 °C.

extracted from a CAD model of the mixer. 7.5 cm and 50 cm of the surrounding pipe was also modelled before and after the mixer respectively. A picture of the CFD mesh can be seen in Fig. 5. The domain was discretized using 5 758 081 tetrahedral cells. The flow was modelled as an incompressible Newtonian flow and the standard k-ε model was used to model turbulence. While the flow before the mixer is laminar, experimental studies have shown that the flow inside SMX mixers are only laminar for Re<10 (pipe Reynolds number) [14]. The incompressibility assumption should be valid as the Mach number of the simulations are 0.001 and the acceptable limit is typically 0.3 – thus compressibility effects are negligible [15].

First, a steady-state solution was simulated for the N_2, entering the domain at 35 L/min at 350 °C (corresponding to 20 L_N/min). Streamlines, visualizing the flow of N_2 through the mixer can be seen in Fig. 6.

After a steady state solution was reached, a transient run with a time step of 0.001 s was made where CO_2 entered the domain from a capillary after the mixer at 7.43 mL/min. To evaluate the mixing, the surface weighted mole fraction of CO_2 was sampled every time step at different planes downstream of the mixer.

The surface weighted mole fraction is used to calculate the uniformity index, defined by Weltens et al. [16] as:

$$\gamma = 1 - \frac{1}{2}\left(\sum_{i=1}^{n} \frac{A_i}{A_{tot}} \cdot \frac{|\psi_i - \psi_{avg}|}{\psi_{avg}}\right) \tag{8}$$

where γ [−] is the uniformity index, A_i [m^2] is the area for segment i with local state variable ψ_i [−] (e.g. concentration), A_{tot} [m^2] is the total area and ψ_{avg} [−] is the area weighted average state variable value.

4. Results and discussion

The results are divided into three distinct parts. Firstly, results showing various outputs from the CFD model of the mixer; velocity vectors and particle streamlines showing the mixing process are presented. This section also includes concentration profiles from the CFD simulations to aid in analysis of the SCAT results. Secondly, the results from the SCAT experiments are presented, identifying the radial concentration maldistribution and the solution to this problem using the static mixer. Thirdly, results from the axial dispersion calculations for the premixed system and injection-based system are presented.

4.1. CFD results

Fig. 6 shows the streamlines colored by velocity magnitude for the CFD simulation of 20 L_N/min at 350 °C (~35 L/min). It can be seen that before the mixer the flow is highly structured and laminar. At the outlet of the mixer there are velocities upwards of 10 m/s and a strong rotary motion around the axial direction is visible. The reason for the acceleration is the reduction in flow area within the mixer as seen in Figs. 2 and 4 – and as the swirl decays, so does the velocity.

The mixing process can be further examined using velocity vectors. Fig. 7 shows two velocity vector profiles defined just at the rear of the mixer and 3 cm downstream. The velocity vectors are normalized by each vector's magnitude for easy tracking of the flow field and its eddies. The left profile in Fig. 7 shows strong eddy formation in the center of the profile where the injection point is located – facilitating shear thinning of fluid elements and improving mixing. The right profile in Fig. 7 shows that only 3 cm downstream the mixer, the eddies are no longer as apparent. The flow field shows strong rotary motion around the center.

From the CFD simulation, concentration profiles presented in Fig. 8

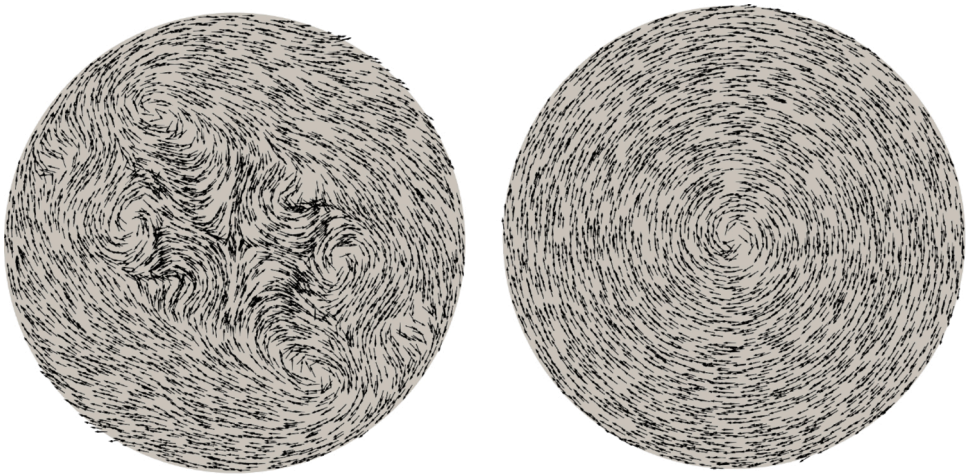

Fig. 7. Velocity vectors, normalized by respective magnitude, defined 0 cm (left) and 3 cm (right) downstream the mixer.

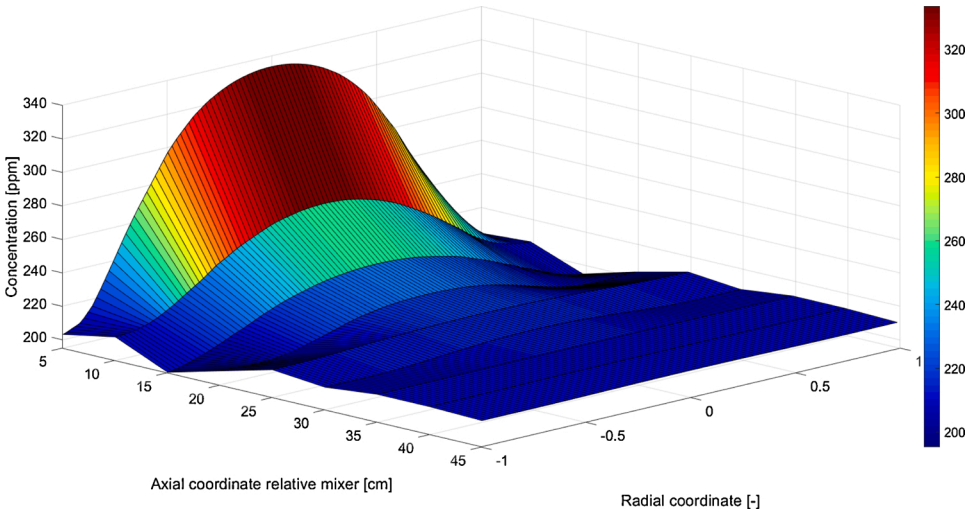

Fig. 8. 3D surface showing the carbon dioxide tracer concentration (z-axis) for various axial positions downstream the mixer (y-axis) as a function of the dimensionless radial coordinate (x-axis).

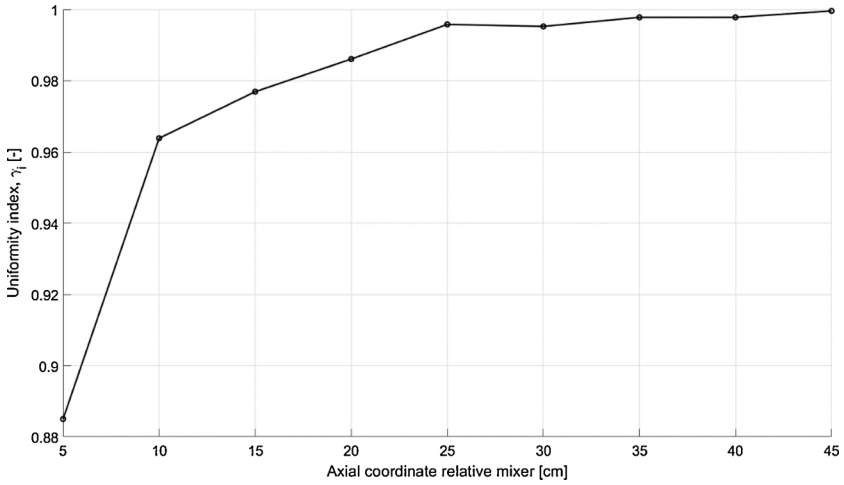

Fig. 9. Uniformity index vs axial coordinate relative the mixer position.

are extracted 5–45 cm downstream the injection point located at the rear of the mixer. It can be seen that close to the mixer, there is still a strong concentration maldistribution with an expected maximum in the center of the pipe where the carbon dioxide tracer is dosed. As the flow moves further downstream the maldistribution is quickly resolved and the profile appears to be completely flat around 35 cm downstream the mixer, where the DOC is placed (Fig. 9).

Equation [8] is used to calculate the axially resolved uniformity index for the concentration profiles extracted from the CFD simulation. The results are presented in Fig. 8. It can be seen that, with respect to the axial coordinate, the mixer rapidly evens out the maldistribution created by the point-injection of carbon dioxide. The mixing process is the fastest up until 25 cm downstream the mixer. After this, the turbulent eddies have likely died out and the driving force for diffusive transport is very low. Hence, with the mixer the DOC could technically be moved roughly 10 cm upstream and still have an equally uniform inlet concentration distribution. However, the length of the entire SCAT bench is still fixed, and the axial dispersion should therefore not decrease.

4.2. Results for SCAT core experiments

The results from the SCAT experiments with 20 L_N/min and 1000 ppm propene step is shown in Fig. 10. To emphasize understanding of the legend, the setups are shown to the right with corresponding color. All catalyst samples are placed 30 cm downstream the injection point. For the cases with a mixer placed upstream the injection point, the rear of the mixer aligns with the injection point. The propene conversion is calculated at the steady state part of the concentration step with error bars corresponding to one standard deviation calculated from the repetitions. Firstly, it can be seen that conversion for the empty SCAT bench itself is virtually non-existent – with some possible reaction occurring at temperatures upwards 550 °C. Hence, it is not possible to conclude or rule out that there is some unwanted oxidation of propene at high temperatures. This could be due to reaction on hot metallic surfaces found after the SCAT bench itself before the analyzers. Secondly, the dashed black line corresponding to the same experiment but with the inserted mixer, also shows no conversion at lower temperature while maybe a little at higher temperatures. In this case, if there is some conversion it is likely due to reactions on hot metallic surfaces after the SCAT bench and not the mixer itself.

While cutting out the DOC core, it was observed that the outer core surfaces retained their catalyst coatings, hence the 25 channels also included four sides with five quarter channels each. This means that the total number of reactive channels increases to 30. Then the reactive area for the core is 9.4 % of that for the complete 400 cpsi cylindrical monolith (319 channels in total). Hence, the conversion in the case of a

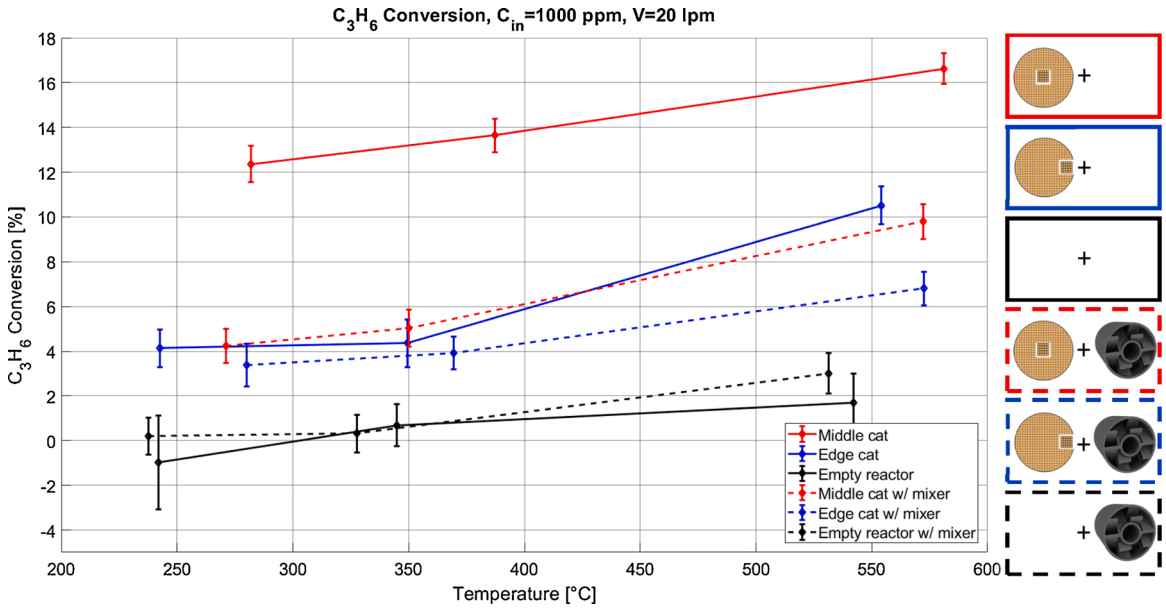

Fig. 10. Conversion vs temperature for reactive core in the middle of the monolith (red solid line), at the edge of the monolith (blue solid line) and empty reactor as baseline (solid black line). Dashed lines correspond to reactive core in the middle of the monolith with inserted mixer (red dashed line), at the edge of the monolith with inserted mixer (blue dashed line) and empty reactor with inserted mixer (solid dashed line). (For interpretation of the references to colour in this figure legend, the reader is referred to the web version of this article).

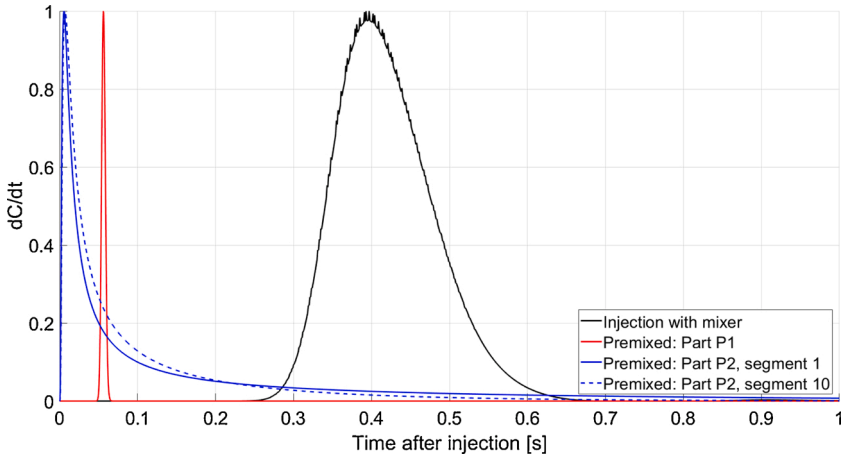

Fig. 11. Time resolved transfer functions for injection-based design with mixer (black solid line), for premixed design part P1 (red solid line), for premixed design part P2 segment 1 (solid blue line) and for premixed design part P2 segment 10 (dashed blue line). Parts P1 and P2 refer to Fig. 1. All curves are normalized by their respective maximum value. (For interpretation of the references to colour in this figure legend, the reader is referred to the web version of this article).

perfect radial concentration distribution should not exceed 9.4 % after light-off and when full conversion (100 %) of propene would be achieved for the complete monolith. Comparing the red and blue solid lines, corresponding to a reactive core in the center and at the edge of the empty monolith, it can be seen that the conversion in the center streamline of the SCAT bench is much higher than that of the edge position. Since the temperatures are similar, this means that differences in conversion result from a radial concentration maldistribution. At lower temperatures, comparing the conversion, there is a three times higher concentration in the middle than at the edge. It is also evident that there is an accumulation of tracer mass in the middle of the SCAT bench pipe, since the conversion is always larger than the theoretical maximum of 9.4 %. By comparing the red and blue dashed lines it can be seen that after inserting the mixer upstream the DOC, the conversion for the two radial positions is identical at the two lower temperatures – if considering the error bars. There are still some differences with mixer at higher temperatures, which could mean that there is still a difference in local inlet concentrations. The results for 40 L_N/min and 100 ppm step changes are very similar to the 1000 ppm case and are therefore not shown here. It should be noted that because there is an accumulation of reactant mass in the case of the center sample without mixer (red solid line), there should be less mass of reactant in at the edge – i.e. the edge sample without mixer should have slightly less conversion than that of the well-mixed case and edge sample (blue dashed line). Since this is not the case it is reasonable to believe that there is not only a maldistribution in the cases without mixer, but that there is an asymmetrical maldistribution. That is, if the edge sample was rotated 180 degrees, its performance might decrease. This would explain why the edge sample without mixer has as good of a performance as the edge sample and well-mixed flow.

4.3. Axial dispersion effect

The transfer functions for each section of the premixed design as well

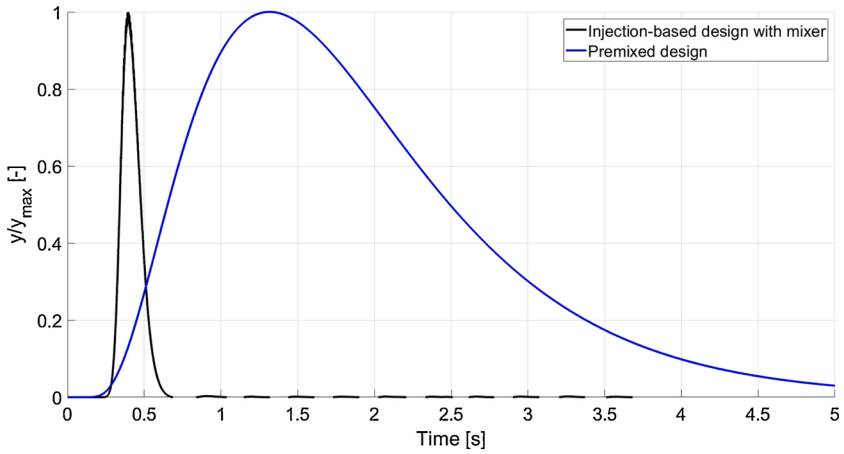

Fig. 12. Response after a Dirac-delta function (instantaneous pulse with unit area) is convoluted with the transfer function of the injection-based design with mixer (black solid line) as well as all transfer function of the premixed design (blue solid line). All curves are normalized by their respective maximum value. (For interpretation of the references to colour in this figure legend, the reader is referred to the web version of this article).

as the injection-based design with mixer is presented in Fig. 11. For Figs. 11 and 12, because of the very different pulse broadening for each design leading to very different amplitude for the curves, to be able to view the curves in the same graph each curve is not normalized with its integral but by its maximum value – forcing the maximum value of all curves to unity. It can be seen that the injection-based design with inserted mixer shows the highest broadening as well as time delay. However, the injection-based transfer function is for the entire system, whereas the transfer function for the premixed design is shown as its components. The turbulent pipe (part P1) shows as expected very little axial dispersion due to the flat velocity profile as a result of high velocity. Lastly, it can be seen that each laminar segment (part P2) gives rise to very little delay. However, the axial dispersion coefficient is the largest for this part. Comparing part P2, segment 1 and part P2, segment 10 it can be seen that the first segment, which is at room temperature has the highest dispersion effect for the premixed design. It should be mentioned that the k-ε turbulence model might not be able to perfectly capture the transition between laminar and turbulent flow. However, the simulation results were in good agreement with the experiments used to develop the mixer and the radial concentration profiles agree with the reactive SCAT experiments. It is possible that the transfer function for the injection-based design would look different with transitional CFD models, however, it is not likely that the results would differ as much so that the premixed design has lower axial dispersion than the injection-based design.

The responses after a Dirac-delta function (instantaneous pulse with unit area) has been convoluted with each SCAT design's overall transfer function as shown in Fig. 12. It can be seen that the response from the injection-based design has far less pulse broadening than the premixed system. The delay between the time of injection and onset of the response at the DOC inlet is also shorter for the injection-based design. The delay and rise time for the premixed system is 1.45 s while it is only 0.4 s for the injection-based system. This is largely due to the shorter distances that the flow is mixed and axial dispersion can occur. Hence, the injection-based system is far superior when it comes to maintaining the transient nature of the experiments. It should be mentioned that unless the SCAT bench will be applied for performing transient experiments, the axial dispersion is of lesser importance. Furthermore, unless high speed sampling is being used (f>>1 Hz), the axial dispersion might appear as indistinguishable for the two systems, as both Dirac-pulse responses in Fig. 12 have reached their maximum value after around 1 s.

5. Conclusions

A method for identifying radial concentration maldistribution in synthetic catalyst activity test benches, where spatially resolved concentration measurements are not available, was developed. The developed methodology was successfully tested for an injection-based SCAT bench and the results showed that there indeed was an accumulation of reactants in the centerline near the injection point. To resolve the radial concentration maldistribution a static mixer was designed, 3D-printed and inserted upstream the test sample. Once repeating the experiments, it was concluded that the mixer managed to resolve the concentration profile while simultaneously not causing reaction disturbances. The resulting increased axial dispersion from the turbulence created by the static mixer was evaluated using a 3D CFD model in Ansys Fluent 19. The axial dispersion of the injection-based SCAT bench was compared to a premixed SCAT bench, where no radial maldistributions occur, through classical Aris-Taylor calculations. The results from the axial dispersion calculations showed that the injection-based design with the use of a static mixer is far superior to the premixed design – both with regards to pulse broadening but also time delay. This is highly desirable for modelling studies towards zero emission exhaust aftertreatment. However, if transient experiments are not required or if the sampling frequency of the analyser is not fast enough – the difference in axial dispersion is inconsequential. Nevertheless, fulfilment and verification of reactor inlet conditions is always of utmost importance.

Author's statement

All authors have participated in (a) conception and design, or analysis and interpretation of the data; (b) drafting the article or revising it critically for important intellectual content; and (c) approval of the final version.

This manuscript has not been submitted to, nor is under review at, another journal or other publishing venue.

The authors have no affiliation with any organization with a direct or indirect financial interest in the subject matter discussed in the manuscript

The following authors have affiliations with organizations with direct or indirect financial interest in the subject matter discussed in the manuscript:

Declaration of Competing Interest

The authors report no declarations of interest.

Acknowledgements

All project members, Patrik Wåhlin at Chalmers University of

Technology as well as the technical staff at Johnson Matthey are deeply acknowledged for their help with performing and analyzing the experiments. Huge thanks to RISE Sweden for printing and providing the project with the finalized mixer. The Swedish Energy Agency (FFI Project 42814-1) is acknowledged for financial support.

References

[1] Z.I. Önsan, A.K. Avci, Monolith reactors. Multiphase Catalytic Reactors - Theory, Design, Manufacturing, and Applications, John Wiley & Sons, 2016.
[2] D.E. Webster, 25 Years of Catalytic Automotive Pollution Control: A Collaborative Effort, 2001, pp. 33–38.
[3] C. Depcik, A. Srinivasan, One + one-dimensional modeling of monolithic catalytic converters, Chem. Eng. Technol. 34 (12) (2011) 1949–1965.
[4] B. Lundberg, J. Sjoblom, Å Johansson, B. Westerberg, D. Creaser, Parameter estimation of a DOC from engine rig experiments with a discretized catalyst washcoat model, SAE Int. J. Engines 7 (2) (2014) 1093–1112.
[5] S.Y. Joshi, M.P. Harold, V. Balakotaiah, Low-dimensional models for real time simulations of catalytic monoliths, AIChE J. 55 (7) (2009) 1771–1783.
[6] R.E. Hayes, A. Fadic, J. Mmbaga, A. Najafi, CFD modelling of the automotive catalytic converter, Catal. Today 188 (1) (2012) 94–105.
[7] R.J. Berger, F. Kapteijn, J.A. Moulijn, G.B. Marin, J. De Wilde, M. Olea, et al., Dynamic methods for catalytic kinetics, Appl. Catal. A Gen. 342 (1) (2008) 3–28.
[8] S. Soltani, R. Andersson, B. Andersson, Time resolution in transient kinetics. Inverse problems and applications, Springer Proceedings in Mathematics & Statistics (2015) 81–96.
[9] M. Singh, P. Anderson, H. Meijer, Understanding and optimizing the SMX static mixer, Macromol. Rapid Commun. 30 (2009) 362–376.
[10] D. Rauline, P.A. Tanguy, J.-M. Le Blévec, J. Bousquet, Numerical investigation of the performance of several static mixers, Canad. J. Chem. Eng. 76 (3) (1998) 527–535.
[11] S. Jegatheeswaran, F. Ein-Mozaffari, J. Wu, Process intensification in a chaotic SMX static mixer to achieve an energy-efficient mixing operation of non-newtonian fluids, Chem. Eng. Process. Process. Intensif. 124 (2018) 1–10.
[12] D. Rossi, L. Gargiulo, G. Valitov, A. Gavriilidis, L. Mazzei, Experimental characterization of axial dispersion in coiled flow inverters, Chem. Eng. Res. Des. 120 (2017) 159–170.
[13] B. Massey, Mechanics of fluids, in: e_library TF (Ed.), Mechanics of Fluids. 1, Taylor & Francis, 2006, p. 254.
[14] S. Liu, A.N. Hrymak, P.E. Wood, Design modifications to SMX static mixer for improving mixing, AIChE J. 52 (1) (2006) 150–157.
[15] B. Andersson, R. Andersson, L. Håkansson, M. Mortensen, R. Sudiyo, B. van Wachem, Computational Fluid Dynamics for Engineers, Cambridge University Press, Cambridge, 2011.
[16] H. Weltens, H. Bressler, F. Terres, H. Neumaier, D. Rammoser, Optimisation of Catalytic Converter Gas Flow Distribution by CFD Prediction, SAE International, 1993.